The diel cycle of NH3 observed from the FY-4A Geostationary Interferometric Infrared Sounder (GIIRS)

Lieven Clarisse, Martin Damme, Daniel Hurtmans, Bruno Franco, Cathy Clerbaux, Pierre-françois Coheur

Geophysical Research Letters

RESEARCH LETTER
10.1029/2021GL093010

The Diel Cycle of NH_3 Observed From the FY-4A Geostationary Interferometric Infrared Sounder (GIIRS)

Lieven Clarisse[1], Martin Van Damme[1], Daniel Hurtmans[1], Bruno Franco[1], Cathy Clerbaux[1,2], and Pierre-François Coheur[1]

[1]Université libre de Bruxelles (ULB), Spectroscopy, Quantum Chemistry and Atmospheric Remote Sensing (SQUARES), Brussels, Belgium, [2]LATMOS/IPSL, Sorbonne Université, UVSQ, CNRS, Paris, France

Key Points:

- We report the first observations of atmospheric NH_3 from the geostationary satellite FY-4A GIIRS over Asia
- The potential of GIIRS to reveal the diurnal and nocturnal variations of NH_3 total columns is demonstrated over two sites
- To better exploit geostationary data, improved temperature profiles and knowledge on the vertical NH_3 distribution is needed

Supporting Information:

Supporting Information may be found in the online version of this article.

Correspondence to:

L. Clarisse,
lieven.clarisse@ulb.be

Citation:

Clarisse, L., Van Damme, M., Hurtmans, D., Franco, B., Clerbaux, C., & Coheur, P.-F. (2021). The diel cycle of NH_3 observed from the FY-4A Geostationary Interferometric Infrared Sounder (GIIRS). *Geophysical Research Letters*, *48*, e2021GL093010. https://doi.org/10.1029/2021GL093010

Received 17 FEB 2021
Accepted 5 JUN 2021

Abstract Limiting excess atmospheric ammonia (NH_3) is one of the great challenges for humanity in the 21st century but can only be achieved with adequate monitoring means in place. Here, we report the first NH_3 measurements from the Geostationary Interferometric Infrared Sounder (GIIRS) onboard the Chinese FY-4A satellite. The instrument scans almost all of Asia 10 times per day. We show that GIIRS' unprecedented temporal sampling can be exploited to measure diurnal and nocturnal variations of NH_3 and demonstrate this on two case studies over Punjab and the North China Plain. Day–night variations are found to be almost absent in winter, but can reach a factor 2–3 in the warmer months. These case studies are very promising given the future landscape of geostationary sounders, but also show that improved knowledge on lower tropospheric air temperatures and the vertical profile of NH_3 is key to better exploit their measurements.

Plain Language Summary To reduce the worldwide concentrations of ammonia (NH_3) in the air is one of the great challenges for humanity in the 21st century, but this can only be achieved with stringent policies in place, and with the support of accurate and frequent measurements. In this paper, we report the first ammonia measurements from the Geostationary Interferometric Infrared Sounder (GIIRS) onboard the Chinese FY-4A satellite. The satellite is positioned above Indonesia and measures almost all of Asia 10 times per day. We show that GIIRS' measurements can be used to measure ammonia both during day and night. We look into more detail at two locations, over Punjab (Pakistan) and the North China Plain. Day-night variations are found to be almost absent in the colder months, but can reach a factor 2–3 in the warmer months. These case studies are very promising given the future landscape of geostationary sounders, but demonstrate also that improved knowledge on the air temperature at the surface and the behavior of ammonia at higher altitudes will result in more accurate ammonia measurements.

1. Introduction

As the atmosphere's primary base and one of the main reactive nitrogen compounds, ammonia (NH_3) plays a key role in our atmosphere and the global nitrogen cycle (Fowler et al., 2013). Emitted in excess, NH_3 can lead to a dramatic loss of biodiversity and deterioration of water, soil and air quality (Bauer et al., 2016; Bobbink et al., 2010; Sutton, Bleeker, et al., 2013). Unlike other primary gaseous pollutants, such as the acidifying NO_x and SO_2 (Aas et al., 2019; Georgoulias et al., 2019), concentrations of NH_3 are steadily increasing in large parts of the world (Sutton et al., 2020; Van Damme et al., 2021). NH_3 has stayed under the radar for long, partially as a result of the historic dearth of measurements. Fortunately, thanks to the availability of new and cheaper techniques, large measurement networks of ground-based stations are gradually put in place (Nair & Yu, 2020; Viatte et al., 2021). In addition, since over a decade, satellites equipped with high-resolution infrared spectrometers offer an unprecedented temporal and spatial sampling of the global NH_3 distributions, which has led to important progress in our understanding of its local to global emission and deposition fluxes and how these are evolving over time (e.g., Cao et al., 2020; Kharol et al., 2018; Van Damme et al., 2018; Warner et al., 2017). There are currently several polar-orbiting satellites that provide global coverage up to twice a day at spatial resolutions above 10 km. These include IASI at 9.30 a.m./p.m. (Whitburn et al., 2016), AIRS (Warner et al., 2016) and CrIS at 1.30 a.m./p.m. (Shephard et al., 2020), and TANSO-FTS (Someya et al., 2020) at 1.00 a.m./p.m.

The diel (day and night) cycle of NH_3 can provide valuable information on its sources, surface exchanges, deposition, gas-particle partitioning and transport, and how each of these are affected by meteorological conditions (Kuang et al., 2020; Schulte et al., 2020). Its understanding is also critically needed to improve atmospheric models (Cao et al., 2020; Lonsdale et al., 2017; Zhu et al., 2015). When talking about daily variations, it is important to differentiate between emissions, surface concentrations and total columns. (i) Emissions of NH_3 typically exhibit a maximum during the day, due to increased temperature-driven volatilization (Sutton, Reis, et al., 2013) and the presence of diurnal sources (Chang et al., 2016). (ii) By contrast, there are large variations in the time when the minimum and maximum surface concentrations are reached (see Tevlin et al. (2017) for an overview). A key element that drives their cycle is the vertical mixing that occurs within the planetary boundary layer (PBL) which determines to what extent NH_3 remains trapped at the surface or undergoes transport to higher altitudes (e.g., Saylor et al. 2010; Walker et al., 2006). (iii) Some diurnal measurements of NH_3 total columns are available (Dammers et al., 2017; Kutzner et al., 2020; W. Wang et al., 2020) from ground-based spectroscopy. These show that the daily evolution of the column can also significantly differ (and even anti-correlate) from the variations at the surface. No measurements of NH_3 total column variations during nighttime have been reported. Furthermore, until now, it is almost uniquely daytime satellite measurements that have been exploited, as nighttime measurements typically come with larger retrieval uncertainties (Van Damme et al., 2014).

The geostationary meteorological satellite FengYun-4 was brought into orbit on 11 December 2016 around the Earth at an altitude of 35,786 km above the equator at 104.7° E. On board it carries several instruments including the Geostationary Interferometric Infrared Sounder (GIIRS) (Hua et al., 2018; Shang et al., 2019; Yang et al., 2017). Its coverage includes almost all of Asia, which is scanned 10 times per day (starting at 0, 2, 4, 6, 8, 10, 12, 14, 20, and 22 h UTC) (Q. Zhang et al., 2019). GIIRS measures the Earth's infrared radiation in two bands at 700–1130 cm^{-1} and 1650–2250 cm^{-1} at a sampling rate of 0.625 cm^{-1}. The noise varies between 0.25 and 0.35 K at 280 K between 900 and 1000 cm^{-1}. The spatial resolution is 16 km. GIIRS is the first interferometer on board a geostationary satellite and its main goal is the provision of temperature and humidity profiles for improved weather forecasts (Cai et al., 2020; Smith et al., 2020). However, with a spectral resolution and range similar to that of CrIS, GIIRS is in principle capable of measuring trace gases as well, and with its 10 overpasses per day could have the potential of capturing the full diel cycle of NH_3 total columns.

In this paper, we report the first NH_3 observations from GIIRS (Section 2) and subsequently introduce a dataset of GIIRS-derived NH_3 columns (Section 3). In Section 4, we provide monthly climatologies of the daily variations of GIIRS-derived columns, in particular focusing on two distinct locations with year-round high NH_3 columns. We use these case studies also to illustrate dependencies on auxiliary data and sensitivity to retrieval assumptions. We conclude with an outlook (Section 5).

2. Absorption and Emission

Two example spectra observed over the North China Plain (NCP) are shown in Figure 1. The top panel presents a spectrum (blue) that was measured by GIIRS in an afternoon overpass on a summer's day. This spectrum was fitted with an inverse model (red), to enable visualizing the NH_3 spectral contribution (orange and black), similarly as in Clarisse et al. (2010). The two largest absorption features of NH_3 in the longwave infrared, around 930 and 965 cm^{-1} show up with a contribution between 2 and 4 K, in addition to several other smaller enhancements, which altogether amply demonstrate the capability of GIIRS to measure NH_3. This fit also illustrates the fact that no large spectral miscalibrations exist in the L1 data (this is not the case for spectra recorded prior to November 2019, which have a noticeable wavenumber shift; see also Smith et al. (2020)). A large NH_3 column combined with a large thermal contrast (TC), as is the case here, represent ideal conditions for retrieving NH_3 columns from satellite measurements.

We briefly recall the concept of TC as it is important for what follows and refer to Clarisse et al. (2010) and Bauduin et al. (2017) for in-depth discussions. TC is the temperature difference between the surface and the lowermost atmospheric layer, where most NH_3 is located. As a consequence of the fact that Earth's surface heats up and cools down more quickly than the atmosphere, it typically becomes positive after sunrise and negative in the evening and at night. For a given NH_3 column, large TCs result in larger spectral signatures, and thus smaller retrieval uncertainties. On the other hand, when the TC is negative, NH_3 can be observed

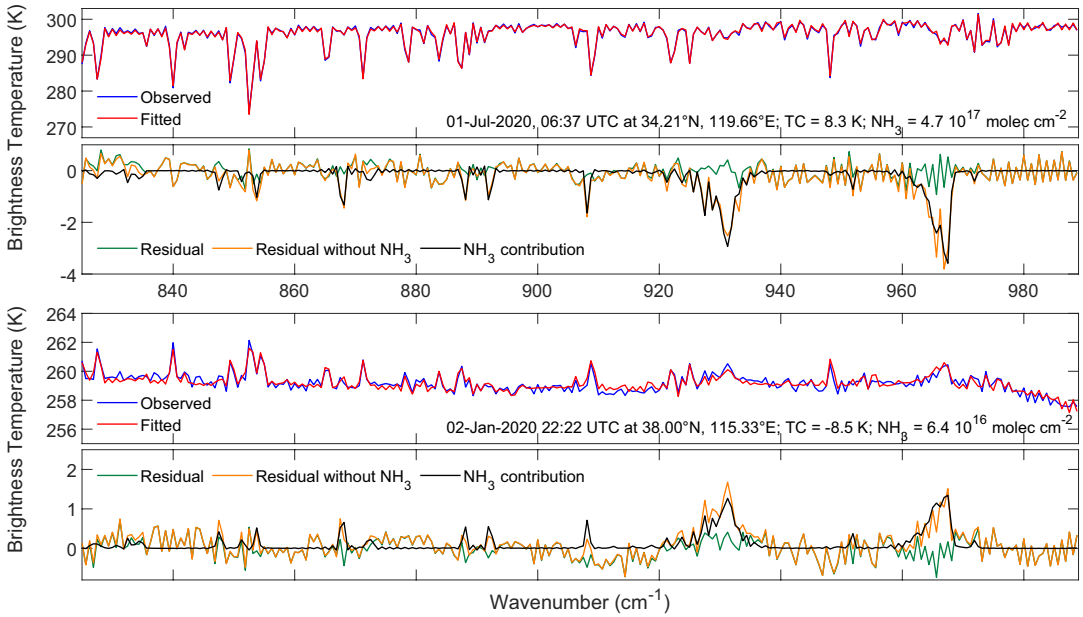

Figure 1. GIIRS spectra (blue) observed over the North China Plain in summer (top) and winter (bottom). The red spectra were calculated with a forward model and were adjusted to best match the observed spectra. The difference between observed and fitted is shown in green. When the NH_3-contribution (black) is removed from the simulations, the orange residuals are obtained.

in emission instead of absorption. This case is illustrated in the bottom panel of Figure 1, which shows a spectrum observed in the early morning in winter. As the air (and thus the NH_3 gas) is in this case warmer than the surface, the NH_3 layer emits more radiation than it absorbs, providing favorable conditions for its measurement. TC thus determines the sign and the dynamic range over which the NH_3 spectral signature can vary, and therefore the retrieval uncertainty.

3. Retrieval

For this study, we have adapted the fast NH_3 retrieval approach originally developed for IASI, which has been detailed in a series of papers (Franco et al., 2018; Van Damme et al., 2017, 2021; Whitburn et al., 2016). Apart from instrument-specific aspects (such as the spectral range), the retrieval procedure is identical to version 3 of the IASI retrieval outlined in the last two papers.

At the heart of the retrieval is the hyperspectral radiance index (HRI), which quantifies the NH_3 spectral signature. This index is normalized to have a mean of zero and a standard deviation of one in the absence of observable NH_3, and its sign can be both positive or negative depending on whether NH_3 is observed in absorption or emission. The HRI depends on the NH_3 abundance, but also on the temperature profile and other parameters (like viewing angle). The algorithm converts HRIs to columns with a neural network that takes into account all these dependencies. The neural network was trained with a large library of synthetic spectra that were simulated with random, but representative NH_3 columns and auxiliary variables. The state of the atmosphere at the overpass time and place of GIIRS were obtained from the ERA5 reanalysis (Hersbach et al., 2020). An important aspect of any NH_3 retrieval is the assumption that is made on the shape of the NH_3 vertical profile. NH_3 is emitted mainly at the surface and has an atmospheric lifetime of a couple of hours (Van Damme et al., 2018); it is therefore largely confined to the PBL. To model the resulting vertical profile, the retrieval assumes a Gaussian function with a maximum at the surface and a spread σ equal to the ERA5 modeled PBL height. This profile is assumed over all land surfaces; over ocean a profile that peaks at 1.4 km is assumed. Fortunately, small uncertainties in the assumed profile generally do not majorly affect the retrieved column. In daytime conditions for instance, the difference in the retrieved column assuming a perfectly mixed PBL of 1 km compared to one of 0.1 or 2 km is about 25% (Whitburn et al., 2016).

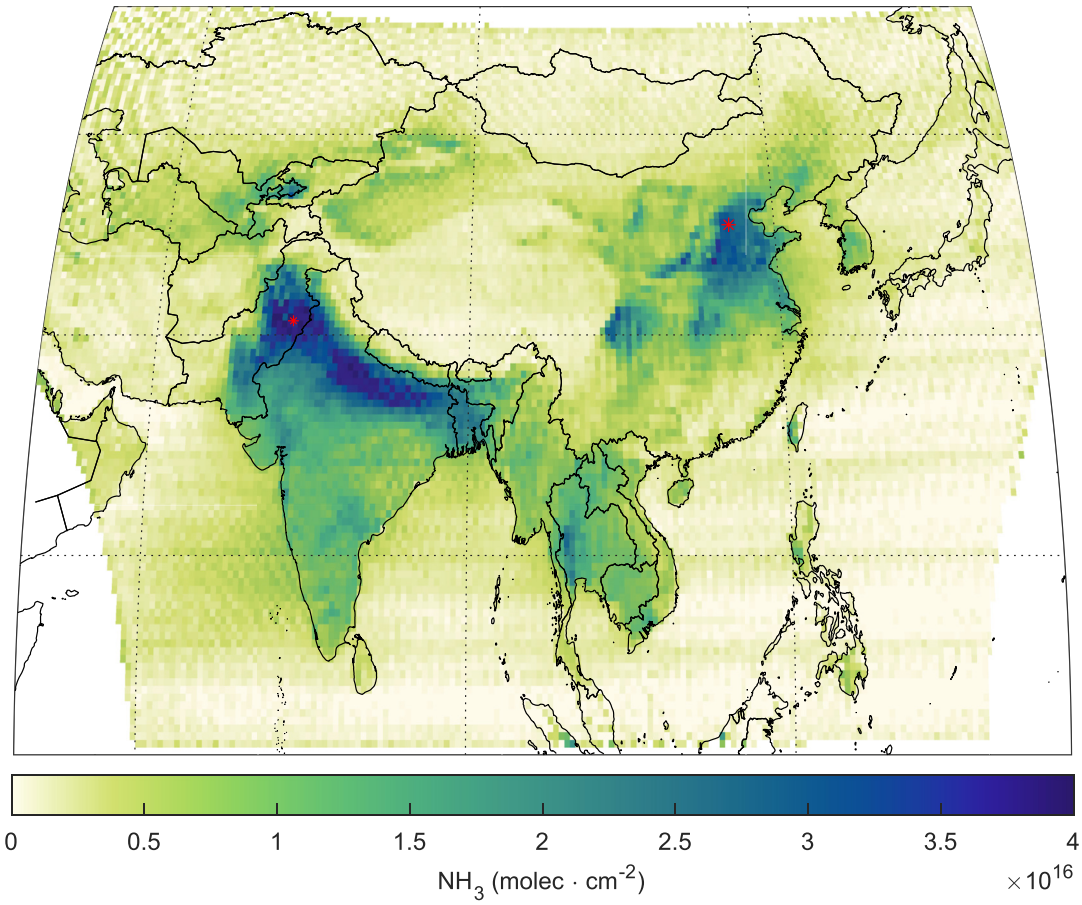

Figure 2. November 2019 to October 2020 average of GIIRS-derived NH_3 columns on a 0.5° × 0.5° grid. Due to the cloud or sensitivity filter (see text), certain periods of the day or year might locally be under/overrepresented in this average. The red stars indicate the locations of the two sites analyzed in Section 4 and Figure 4 (30° N, 73° E for Pakistan and 38° N, 115.5° E for China).

A postfilter was applied which removes cloudy observations and those measurements with limited sensitivity to NH_3 due to low TC. These were selected based on having a conversion factor between the HRI and the column in excess of $10 \cdot 10^{15}$ molec.cm^{-2}. In addition, as in previous work on IASI, a retrieval uncertainty was estimated for each individual pixel, by propagation of the uncertainty of the individual input parameters. The uncertainty on σ was set to 25%. For the detection of clouds, a dedicated neural network was trained here from collocated IASI–GIIRS observations and the IASI L2 cloud product. This network, which takes as input a handful of GIIRS channels, was set up to select scenes without clouds.

The retrieval has been performed on a complete year of GIIRS observations, from November 2019 to October 2020, and the resulting dataset is with this publication made available. The average of all observations measured in this period is shown in Figure 2 and qualitatively exhibits a good agreement with the IASI distributions (Van Damme et al., 2018). Note that the edges of the seven latitudinal bands in which GIIRS scans the entire area can be discerned in the NH_3 distribution, hinting toward a residual artifact in the L1 data. The resulting biases are however very small in comparison to the actual variability of the columns.

We intercompared GIIRS-derived columns with v3 of the IASI NH_3 dataset (Van Damme et al., 2021), collocated within 2 km and 15 min, and as a whole found a regression slope of 1.14, negligible bias and a correlation coefficient of $R^2 = 0.67$ (see Supporting information S1). Possible reasons for the non-unit slope include instrument calibration, the HRI calculation, treatment of the surface temperature, systematic biases in the neural networks and the different viewing geometries.

4. Diel Cycle

Figure 3 shows the diel cycle observed from GIIRS during January, April, and July, representative for the distributions respectively seen in October–February, March–May, and June–September. A clear seasonal cycle is visible, with a maximum in April–July, consistent with IASI observations (Van Damme et al., 2015). We also observe a more pronounced diel cycle in April/July than in January. Due to the postfilter, the coverage of the NH_3 measurements varies greatly as a function of the time of the day, time of the year and the location. Clouds are unfortunately year-round prevalent in south(east) China and Southeastern Asia. The situation is especially unfavorable in the monsoon season (June–September). In addition, a lot of observations at night, early morning and evening are removed by the sensitivity test.

In what follows we look more into detail into two 1° by 1° areas located in Punjab (Pakistan) and the NCP. These are agricultural intensive regions, with intensively irrigated crops and a high density of livestock (Perrone, 2020; Robinson et al., 2014; Zhan et al., 2021), where some of the largest NH_3 columns in the world are measured (Kuttippurath et al., 2020; Meng et al., 2018; T. Wang et al., 2020; Y. Zhang et al., 2010). Figure 4 shows their monthly averaged diel cycles of the NH_3 column, ERA5 PBL height, HRI, and TC. The TC was calculated as the difference between the temperature measured from GIIRS spectra around 970 cm^{-1} and the temperature corresponding to middle of the PBL. This avoids relying on a dedicated surface temperature retrieval but underestimates its actual value by up to 1–2 K in the dry seasons, and up to 4 K in the wet seasons, because of the water vapor continuum absorption. When fewer than 30 observations are available for a given overpass time, the NH_3 column was obtained by interpolation from the other points of the time series (indicated with hollow squares). This helps to remove potential outliers in the time series. The median uncertainty over all averaged pixels for a given overpass time is shown as a shaded area around the mean value. While this uncertainty includes a random component, it also includes potential sources of bias, related to for example, the vertical profile of NH_3 or the ERA5 temperature profile. For that reason we recommend to exercise care when interpreting the data.

4.1. January

For both sites, the diel cycle is weak in January, consistent with the absence of pronounced diurnal or nocturnal sources at these rural sites in the winter. A slight increase of the columns is observed during nighttime. Such increases have been reported for surface measurements, which are easily explained by the lower nocturnal mixing height, trapping emissions near the surface (Saraswati et al., 2018; Tevlin et al., 2017; Q. Wang et al., 2019). However, as we consider the entire column, the small decreases seen during daytime are more likely due to small biases in the assumed vertical NH_3 profile, the PBL height or the vertical temperature profiles. In January, the diel cycle is captured almost completely, thanks to favorable measurement conditions both during night and day. Ranging between −6 and 7 K, the TCs are sufficiently large to provide sensitivity to the PBL at all times of the day except around dawn and dusk. This is when the HRI and TC cross the zero mark and the time of the day when all sensitivity to PBL NH_3 is lost, irrespective of the magnitude of the column.

4.2. April

With increasing temperatures, and with the growing season well underway, much larger NH_3 columns are observed during April. Columns over Punjab are double those over the NCP, even though emissions are estimated to be lower. This apparent contradiction was attributed to the higher concentrations of the neutralizing NO_x and SO_2 compounds over the NCP, leading to a shorter atmospheric lifetime of NH_3 (Liu et al., 2018; T. Wang et al., 2020). Just as in January, the HRI and TC undergo a synchronous cycle in April, alternating between negative and positive values, and providing favorable measurement conditions at all times of the day except during twilight. The outlying NH_3 column (much below the average) in April near 18:00 in the NCP results likely from a retrieval artifact. As can be seen, the HRI in this case is very close to zero. Assuming no abrupt changes in the NH_3 column, this either points to very low measurement sensitivity or to a situation where emission and absorption cancel each other out in different parts of the atmosphere. In either case, this renders the retrieval from a theoretical standpoint ill-defined. In the majority of cases the postfilter takes care of removing such measurements. However, the thermal conditions as

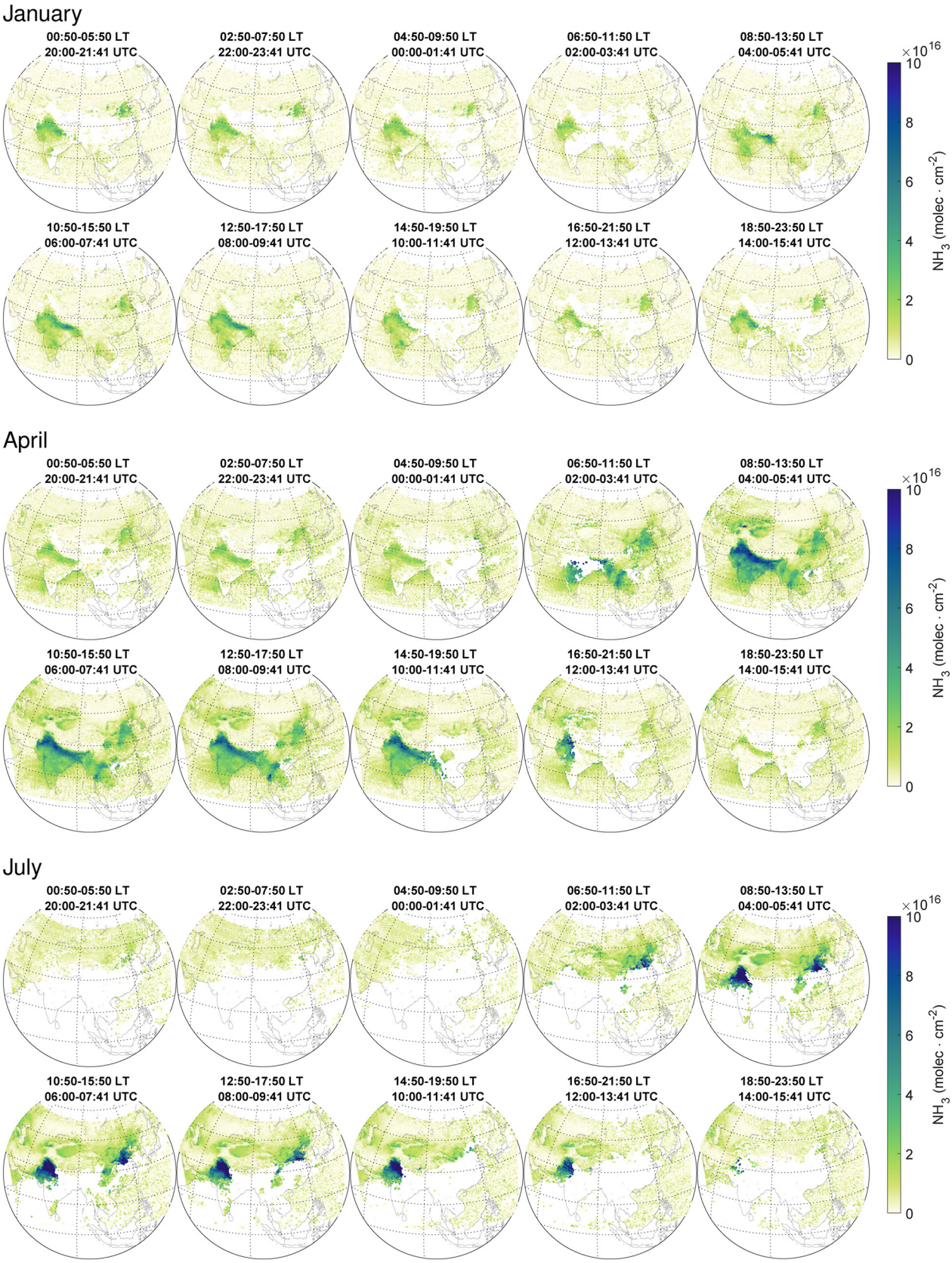

Figure 3. Monthly NH_3 averages for each of the 10 GIIRS overpass times for the months of January, April, and July.

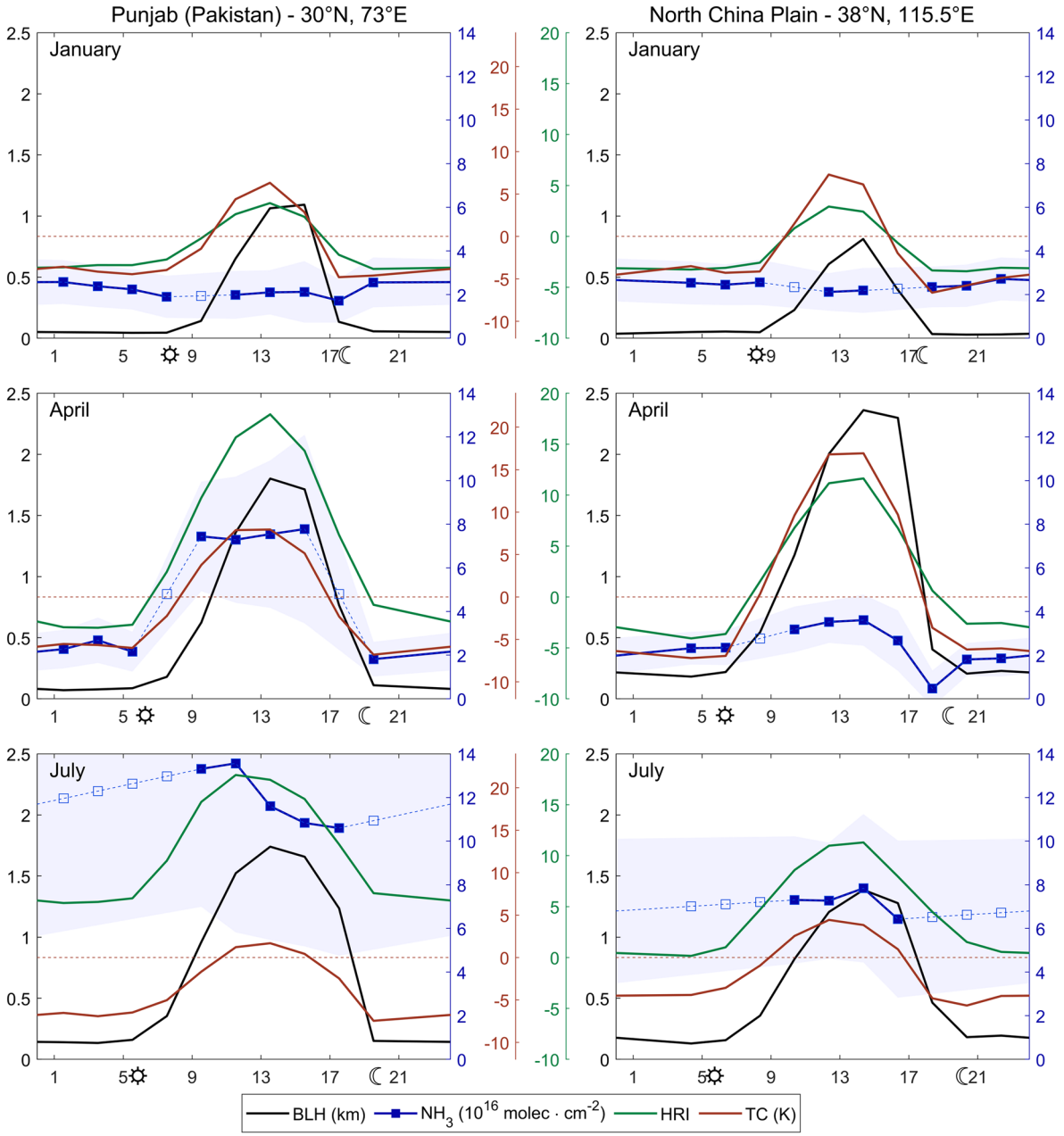

Figure 4. Diurnal cycle of NH_3 (blue) over 1° by 1° areas in Punjab, Pakistan (left) and the North China Plain (right). Data represented with open squares were obtained through interpolation (see text). Shown are also the ERA5 PBL height (black), the TC (dark red), and the HRI (green). The shaded area represent the median uncertainty for a given overpass time. The time axis is in local time (calculated from the longitude) and includes the time sunrise and sunset on the 15th of each month.

provided within ERA5, coupled with the assumed NH_3 vertical profile, are apparently such that a number of these measurements slipped through the net of the postfilter.

A much larger diel cycle is observed in April as compared to January, especially in Punjab with a column more than three times larger during day than at night. Similarly high ratios, with daytime maximums, have been observed in the diel variations of total columns over Paris (Kutzner et al., 2020) and in a rural area in the Netherlands (Dammers et al., 2017). There are a number of factors which explain such large day-night variations. (i) During day, agricultural practices and animal activity (Aarnink et al., 1996) are enhanced. (ii) NH_3 emissions from plants and soils increase during the day due to meteorological factors (Schulte

et al., 2020). Emissions exhibit in particular an up to exponential increase with temperature (Ernst & Massey, 1960; Schjoerring et al., 1998; Sutton, Reis, et al., 2013; Tevlin & Murphy, 2019; L. Zhang et al., 2010), making it an important driver both for the seasonal and the diel emission cycle. While day–night temperature differences (between 15 and 22 K) are not much larger in April than in January, surface temperatures are some 10–15 K larger in April, and via the exponential dependence have a much larger relative effect (Hempel et al., 2016). In addition, during daytime, relative humidity is on average lower and wind speed on average higher than at night, two factors which again favor daytime emissions (Meng et al., 2018; Olesen & Sommer, 1993; Tevlin et al., 2017; Wentworth et al., 2016). (iii) At night, temperatures are lower, humidity levels higher, thereby favoring the conversion of NH_3 gas to particulate. The reverse process may contribute to daytime enhancements (Kutzner et al., 2020; Meng et al., 2018; Saylor et al., 2010; Tevlin et al., 2017). (iv) Finally, nocturnal columns could be underestimated in the retrieval as a result of the vertical profile assumption. The observed negative HRIs are compatible with the sign of the TC, demonstrating that most of the NH_3 column is indeed located near the surface as assumed by the retrieval. However, it cannot be excluded (see below) that compared to the assumed profile, a relative larger portion of the NH_3 column is situated higher up. In this case, the higher and colder parts of the column absorb radiation and therefore cancel out some of the spectral emission at night.

The variations in the diel cycles found here are larger than those typically found for surface concentrations. While NH_3 concentrations are expected to increase during daytime due to increased emissions and also evaporation of ammonium-containing aerosols, the larger boundary layer prevents a large buildup of NH_3 near the surface. For example, in a rural site in the NCP, surface concentrations vary only between 25 and 40 ppb in April, with the maximum reached in the morning due to the evaporation of dew and guttation droplets (Kuang et al., 2020; Wentworth et al., 2016). For other sites in Asia, even smaller differences are reported (Datta et al., 2012; Saraswati et al., 2018; Saylor et al., 2010; S. Wang et al., 2015). In addition, surface concentrations reported in the winter are often only just below those in April (e.g., Kuang et al., 2020; S. Wang et al., 2015). At night, mixing layers in the two months are also of comparable magnitude, and assuming that most NH_3 is located in the PBL, this implies that columns should be of similar magnitude too at night, what is consistent with what is observed here.

4.3. July

July is the month when some of the highest columns are measured for both sites, but unfortunately only 4 or 5 of the 10 overpasses have enough measurements for obtaining meaningful averages, so that little can be said on the diel cycle. In what follows we explore the reasons for the poor measurement conditions.

The first thing to note is that the temperatures of both the surface and the air (not shown) vary little (between 7 and 10 K) throughout the day and night, much smaller than in the January/April months. Smaller day–night variations entail a smaller dynamic range of the TC, as observed clearly in Figure 4, and inherently worsen the conditions for NH_3 detection by GIIRS.

For Punjab, TCs are mostly negative, only just reaching positive numbers around noon. At night, a TC is observed around −6 K. Allowing for the underestimation of the TC by an average of 4 K in this humid month, this puts the actual TC close to zero. This explains why the corresponding measurements are removed by the retrieval postfilter. However, we observe a mean HRI of about five during the night, which suggests a positive TC. A likely explanation is that the NH_3 vertical profile for this site, at this time of the year, is significantly different from the assumed profile at night. Recall that the retrieval assumes that the majority (about 68%) of the NH_3 column is located within the PBL, as supported by several studies (Dammers et al., 2017; Guo et al., 2021; Sun et al., 2015; Tevlin et al., 2017). However, in the evening just after the collapse of the PBL, NH_3 is likely to remain present in the residual layer for several hours (see also Kuang et al., 2020; Lonsdale et al., 2017). Given the relative longer lifetime of NH_3 in the Indo-Gangetic Plain, and the abundance of NH_3 in the daytime summer column, this could explain the positive HRIs observed for Punjab during the night. The measurements with a positive HRI that were removed by the postfilter could in principle be exploited by using a more appropriate vertical profile in the retrieval. Also note that during daytime, elevated free-tropospheric NH_3 layers can occur, as illustrated in a recent aircraft campaign over Baoding (NCP) (Pu et al., 2020).

The diel cycle over the NCP follows a similar pattern as for Punjab in July, but here the absence of sensitivity during the night is obvious with HRI values very close to zero.

5. Outlook

GIIRS is the first geostationary hyperspectral infrared sounder in orbit. As we have shown in this letter, its 10 overpasses provide an unprecedented opportunity to study atmospheric NH_3 and its evolution throughout the day. The availability of so many overpasses per day could also greatly benefit NH_3 modeling and model assimilation (Chen et al., 2021; Z. Wang et al., 2020). Finally, compared to polar orbits, GIIRS has the advantage of revisiting the same footprint every day, which will be most useful for tracking seasonal variations over particular locations, and for validation and intercomparison.

While the presented NH_3 dataset was prepared with great care, improvements are certainly possible. An important improvement could come from the use of temperature profiles directly retrieved from the GIIRS radiances, rather than ERA5 profiles. In addition, a better parametrization of the NH_3 vertical profile as a function of time and place would be highly desirable. This could be achieved by coupling the retrieval with the output of a state of the art tropospheric chemistry model. It is our hope that the presented results will stimulate further research in these directions.

The future landscape of geostationary sounders is looking bright. With a lifetime of 5–7 years, FY-4A is nearing its end, but fortunately, its successor FY-4B is to be launched this year. In addition, Europe is soon to be served with its own geostationary infrared sounder (IRS) onboard the Meteosat Third Generation (MTG) satellite (https://www.eumetsat.int/meteosat-third-generation). IRS is similar to GIIRS but will offer more frequent overpasses and a smaller footprint on ground. Given the results obtained with GIIRS, the arrival of IRS is extremely promising and will no doubt provide fantastic monitoring means of NH_3 over Africa and Europe.

Data Availability Statement

The NH_3 dataset presented in this study is available at https://dx.doi.org/10.5281/zenodo.4540024.

Acknowledgments
We are very grateful to the entire scientific and technical team of GIIRS and FY-4A, the National Satellite Meteorological Center (NSMC, http://www.nsmc.org.cn/NSMC/Home/Index.html) and the China Meteorological Administration (CMA) for making GIIRS possible. We gratefully acknowledge the NSMC for providing open access to the GIIRS data. This research was funded by the F.R.S.-FNRS and the Belgian State Federal Office for Scientific, Technical and Cultural Affairs (Prodex arrangement HIRS). L. Clarisse is Research Associate and M. Van Damme is Postdoctoral Researcher, both supported by the Belgian F.R.S.-FNRS. C. Clerbaux is grateful to CNES for scientific collaboration and financial support.

References

Aarnink, A., van den Berg, A., Keen, A., Hoeksma, P., & Verstegen, M. (1996). Effect of slatted floor area on ammonia emission and on the excretory and lying behaviour of growing pigs. *Journal of Agricultural Engineering Research*, *64*(4), 299–310. https://doi.org/10.1006/jaer.1996.0071

Aas, W., Mortier, A., Bowersox, V., Cherian, R., Faluvegi, G., Fagerli, H., et al. (2019). Global and regional trends of atmospheric sulfur. *Scientific Reports*, *9*(1). https://doi.org/10.1038/s41598-018-37304-0

Bauduin, S., Clarisse, L., Theunissen, M., George, M., Hurtmans, D., Clerbaux, C., & Coheur, P.-F. (2017). IASI's sensitivity to near-surface carbon monoxide (CO): Theoretical analyses and retrievals on test cases. *Journal of Quantitative Spectroscopy & Radiative Transfer*, *189*, 428–440. https://doi.org/10.1016/j.jqsrt.2016.12.022

Bauer, S. E., Tsigaridis, K., & Miller, R. (2016). Significant atmospheric aerosol pollution caused by world food cultivation. *Geophysical Research Letters*, *43*(10), 5394–5400. https://doi.org/10.1002/2016gl068354

Bobbink, R., Hicks, K., Galloway, J., Spranger, T., Alkemade, R., Ashmore, M., et al. (2010). Global assessment of nitrogen deposition effects on terrestrial plant diversity: A synthesis. *Ecological Applications*, *20*(1), 30–59. https://doi.org/10.1890/08-1140.1

Cai, X., Bao, Y., Petropoulos, G. P., Lu, F., Lu, Q., Zhu, L., & Wu, Y. (2020). Temperature and humidity profile retrieval from FY4-GIIRS hyperspectral data using artificial neural networks. *Remote Sensing*, *12*(11), 1872. https://doi.org/10.3390/rs12111872

Cao, H., Henze, D. K., Shephard, M. W., Dammers, E., Cady-Pereira, K., Alvarado, M., et al. (2020). Inverse modeling of NH_3 sources using CrIS remote sensing measurements. *Environmental Research Letters*, *15*(10), 104082. https://doi.org/10.1088/1748-9326/abb5cc

Chang, Y., Zou, Z., Deng, C., Huang, K., Collett, J. L., Lin, J., & Zhuang, G. (2016). The importance of vehicle emissions as a source of atmospheric ammonia in the megacity of Shanghai. *Atmospheric Chemistry and Physics*, *16*(5), 3577–3594. https://doi.org/10.5194/acp-16-3577-2016

Chen, Y., Shen, H., Kaiser, J., Hu, Y., Capps, S. L., Zhao, S., et al. (2021). High-resolution hybrid inversion of IASI ammonia columns to constrain US ammonia emissions using the CMAQ adjoint model. *Atmospheric Chemistry and Physics*, *21*(3), 2067–2082. https://doi.org/10.5194/acp-21-2067-2021

Clarisse, L., Shephard, M. W., Dentener, F., Hurtmans, D., Cady-Pereira, K., Karagulian, F., et al. (2010). Satellite monitoring of ammonia: A case study of the San Joaquin Valley. *Journal of Geophysical Research*, *115*, D13302. https://doi.org/10.1029/2009JD013291

Dammers, E., Schaap, M., Haaima, M., Palm, M., Wichink Kruit, R. J., Volten, H., et al. (2017). Measuring atmospheric ammonia with remote sensing campaign: Part 1 – Characterisation of vertical ammonia concentration profile in the centre of the Netherlands. *Atmospheric Environment*, *169*, 97–112. https://doi.org/10.1016/j.atmosenv.2017.08.067

Datta, A., Sharma, S. K., Harit, R. C., Kumar, V., Mandal, T. K., & Pathak, H. (2012). Ammonia emission from subtropical crop land area in India. *Asia-Pacific Journal of Atmospheric Sciences*, *48*(3), 275–281. https://doi.org/10.1007/s13143-012-0027-1

Ernst, J. W., & Massey, H. F. (1960). The effects of several factors on volatilization of ammonia formed from urea in the soil. *Soil Science Society of America Journal*, *24*(2), 87–90. https://doi.org/10.2136/sssaj1960.03615995002400020007x

Fowler, D., Coyle, M., Skiba, U., Sutton, M. A., Cape, J. N., Reis, S., et al. (2013). The global nitrogen cycle in the twenty-first century. *Philosophical Transactions of the Royal Society B*, *368*(1621), 20130164. https://doi.org/10.1098/rstb.2013.0164

Franco, B., Clarisse, L., Stavrakou, T., Müller, J.-F., Van Damme, M., Whitburn, S., et al. (2018). A general framework for global retrievals of trace gases from IASI: Application to methanol, formic acid, and PAN. *Journal of Geophysical Research – D: Atmospheres*, *123*(24), 13963–13984. https://doi.org/10.1029/2018jd029633

Georgoulias, A. K., van der A, R. J., Stammes, P., Boersma, K. F., & Eskes, H. J. (2019). Trends and trend reversal detection in 2 decades of tropospheric NO_2 satellite observations. *Atmospheric Chemistry and Physics*, *19*(9), 6269–6294. https://doi.org/10.5194/acp-19-6269-2019

Guo, X., Wang, R., Pan, D., Zondlo, M. A., Clarisse, L., Van Damme, M., et al. (2021). Validation of IASI satellite ammonia observations at the pixel scale using in-situ vertical profiles. *Journal of Geophysical Research – D: Atmospheres*, *126*. https://doi.org/10.1029/2020jd033475

Hempel, S., Saha, C. K., Fiedler, M., Berg, W., Hansen, C., Amon, B., & Amon, T. (2016). Non-linear temperature dependency of ammonia and methane emissions from a naturally ventilated dairy barn. *Biosystems Engineering*, *145*, 10–21. https://doi.org/10.1016/j.biosystemseng.2016.02.006

Hersbach, H., Bell, B., Berrisford, P., Hirahara, S., Horányi, A., Muñoz-Sabater, J., et al. (2020). The ERA5 global reanalysis. *Quarterly Journal of the Royal Meteorological Society*, *146*(730), 1999–2049. https://doi.org/10.1002/qj.3803

Hua, J., Wang, Z., Duan, J., Li, L., Zhang, C., Wu, X., et al. (2018). Review of Geostationary Interferometric Infrared Sounder. *Chinese Optics Letters*, *16*(11), 111203. https://doi.org/10.3788/col201816.111203

Kharol, S. K., Shephard, M. W., McLinden, C. A., Zhang, L., Sioris, C. E., OBrien, J. M., et al. (2018). Dry deposition of reactive nitrogen from satellite observations of ammonia and nitrogen dioxide over North America. *Geophysical Research Letters*, *45*(2), 1157–1166. https://doi.org/10.1002/2017gl075832

Kuang, Y., Xu, W., Lin, W., Meng, Z., Zhao, H., Ren, S., et al. (2020). Explosive morning growth phenomena of NH_3 on the North China Plain: Causes and potential impacts on aerosol formation. *Environmental Pollution*, *257*, 113621. https://doi.org/10.1016/j.envpol.2019.113621

Kuttippurath, J., Singh, A., Dash, S., Mallick, N., Clerbaux, C., Van Damme, M., et al. (2020). Record high levels of atmospheric ammonia over India: Spatial and temporal analyses. *The Science of the Total Environment*, *740*, 139986. https://doi.org/10.1016/j.scitotenv.2020.139986

Kutzner, R. D., Cuesta, J., Chelin, P., Petit, J.-E., Ray, M., Landsheere, X., et al. (2020). Diurnal evolution of total column and surface atmospheric ammonia in the megacity of Paris, France, during an intense springtime pollution episode. *Atmospheric Chemistry and Physics Discussions*. https://doi.org/10.5194/acp-2020-782

Liu, M., Huang, X., Song, Y., Xu, T., Wang, S., Wu, Z., et al. (2018). Rapid SO_2 emission reductions significantly increase tropospheric ammonia concentrations over the North China Plain. *Atmospheric Chemistry and Physics*, *18*(24), 17933–17943. https://doi.org/10.5194/acp-18-17933-2018

Lonsdale, C. R., Hegarty, J. D., Cady-Pereira, K. E., Alvarado, M. J., Henze, D. K., Turner, M. D., et al. (2017). Modeling the diurnal variability of agricultural ammonia in Bakersfield, California, during the CalNex campaign. *Atmospheric Chemistry and Physics*, *17*(4), 2721–2739. https://doi.org/10.5194/acp-17-2721-2017

Meng, Z., Xu, X., Lin, W., Ge, B., Xie, Y., Song, B., et al. (2018). Role of ambient ammonia in particulate ammonium formation at a rural site in the North China Plain. *Atmospheric Chemistry and Physics*, *18*(1), 167–184. https://doi.org/10.5194/acp-18-167-2018

Nair, A. A., & Yu, F. (2020). Quantification of atmospheric ammonia concentrations: A review of its measurement and modeling. *Atmosphere*, *11*(10), 1092. https://doi.org/10.3390/atmos11101092

Olesen, J., & Sommer, S. (1993). Modelling effects of wind speed and surface cover on ammonia volatilization from stored pig slurry. *Atmospheric Environment Part A. General Topics*, *27*(16), 2567–2574. https://doi.org/10.1016/0960-1686(93)90030-3

Perrone, D. (2020). Groundwater overreliance leaves farmers and households high and dry. *One Earth*, *2*(3), 214–217. https://doi.org/10.1016/j.oneear.2020.03.001

Pu, W., Guo, H., Ma, Z., Qiu, Y., Tang, Y., Liu, Q., et al. (2020). Aircraft measurements reveal vertical distribution of atmospheric ammonia over the North China Plain in early autumn. *Environmental Chemistry Letters*, *18*(6), 2149–2156. https://doi.org/10.1007/s10311-020-01051-4

Robinson, T. P., Wint, G. R. W., Conchedda, G., Boeckel, T. P. V., Ercoli, V., Palamara, E., et al. (2014). Mapping the global distribution of livestock. *PloS One*, *9*(5), e96084. https://doi.org/10.1371/journal.pone.0096084

Saraswati, Sharma, S. K., & Mandal, T. K. (2018). Five-year measurements of ambient ammonia and its relationships with other trace gases at an urban site of Delhi, India. *Meteorology and Atmospheric Physics*, *130*(2), 241–257. https://doi.org/10.1007/s00703-017-0512-2

Saylor, R. D., Edgerton, E. S., Hartsell, B. E., Baumann, K., & Hansen, D. A. (2010). Continuous gaseous and total ammonia measurements from the southeastern aerosol research and characterization (SEARCH) study. *Atmospheric Environment*, *44*(38), 4994–5004. https://doi.org/10.1016/j.atmosenv.2010.07.055

Schjoerring, J. K., Husted, S., & Mattsson, M. (1998). Physiological parameters controlling plant–atmosphere ammonia exchange. *Atmospheric Environment*, *32*(3), 491–498. https://doi.org/10.1016/s1352-2310(97)00006-x

Schulte, R., van Zanten, M., Rutledge-Jonker, S., Swart, D., Wichink Kruit, R., Krol, M., et al. (2020). Unraveling the diurnal atmospheric ammonia budget of a prototypical convective boundary layer. *Atmospheric Environment*, *249*, 118153. https://doi.org/10.1016/j.atmosenv.2020.118153

Shang, J., Yang, L., Huang, P., Yang, H., Liu, C., Wang, J., et al. (2019). Instrument observation strategy for a new generation of three-axis-stabilized geostationary meteorological satellites from China. *Geoscientific Instrumentation, Methods and Data Systems*, *8*(2), 161–175. https://doi.org/10.5194/gi-8-161-2019

Shephard, M. W., Dammers, E., Cady-Pereira, K. E., Kharol, S. K., Thompson, J., Gainariu-Matz, Y., et al. (2020). Ammonia measurements from space with the Cross-track Infrared Sounder: Characteristics and applications. *Atmospheric Chemistry and Physics*, *20*(4), 2277–2302. https://doi.org/10.5194/acp-20-2277-2020

Smith, W. L., Zhang, Q., Shao, M., & Weisz, E. (2020). Improved severe weather forecasts using LEO and GEO satellite soundings. *Journal of Atmospheric and Oceanic Technology*, *37*(7), 1203–1218. https://doi.org/10.1175/jtech-d-19-0158.1

Someya, Y., Imasu, R., Shiomi, K., & Saitoh, N. (2020). Atmospheric ammonia retrieval from the TANSO-FTS/GOSAT thermal infrared sounder. *Atmospheric Measurment Techniques*, *13*(1), 309–321. https://doi.org/10.5194/amt-13-309-2020

Sun, K., Cady-Pereira, K., Miller, D. J., Tao, L., Zondlo, M. A., Nowak, J. B., et al. (2015). Validation of TES ammonia observations at the single pixel scale in the San Joaquin Valley during DISCOVER-AQ. *Journal of Geophysical Research - D: Atmospheres*, *120*(10), 5140–5154. https://doi.org/10.1002/2014jd022846

Sutton, M. A., Bleeker, A., Howard, C., Bekunda, M., Grizzetti, B., de Vries, W., & Zhang, F. (2013). Our nutrient world: The challenge to produce more food and energy with less pollution. Centre for Ecology and Hydrology (CEH).

Sutton, M. A., Reis, S., Riddick, S. N., Dragosits, U., Nemitz, E., Theobald, M. R., et al. (2013). Toward a climate-dependent paradigm of ammonia emission and deposition. *Philosophical Transactions of the Royal Society B*, *368*(1621), 20130166. https://doi.org/10.1098/rstb.2013.0166

Sutton, M. A., van Dijk, N., Levy, P. E., Jones, M. R., Leith, I. D., Sheppard, L. J., et al. (2020). Alkaline air: Changing perspectives on nitrogen and air pollution in an ammonia-rich world. *Philosophical Transactions of the Royal Society A: Mathematical, Physical and Engineering Sciences*, *378*(2183), 20190315. https://doi.org/10.1098/rsta.2019.0315

Tevlin, A. G., Li, Y., Collett, J. L., McDuffie, E. E., Fischer, E. V., & Murphy, J. G. (2017). Tall tower vertical profiles and diurnal trends of ammonia in the Colorado Front Range. *Journal of Geophysical Research - D: Atmospheres*, *122*(22468–12), 12. https://doi.org/10.1002/2017jd026534

Tevlin, A. G., & Murphy, J. G. (2019). Atmospheric ammonia: Measurements, modeling, and chemistry–Climate interactions. In: *Advances in atmospheric chemistry* (pp. 1–82). World Scientific. https://doi.org/10.1142/9789813271838_0001

Van Damme, M., Clarisse, L., Franco, B., Sutton, M. A., Erisman, J. W., Wichink Kruit, R. J. et al. (2021). Global, regional and national trends of atmospheric ammonia derived from a decadal (2008–2018) satellite record. *Environmental Research Letters*. https://doi.org/10.1088/1748-9326/abd5e0

Van Damme, M., Clarisse, L., Heald, C., Hurtmans, D., Ngadi, Y., Clerbaux, C., et al. (2014). Global distributions, time series and error characterization of atmospheric ammonia (NH_3) from IASI satellite observations. *Atmospheric Chemistry and Physics*, *14*(6), 2905–2922. https://doi.org/10.5194/acp-14-2905-2014

Van Damme, M., Clarisse, L., Whitburn, S., Hadji-Lazaro, J., Hurtmans, D., Clerbaux, C., & Coheur, P.-F. (2018). Industrial and agricultural ammonia point sources exposed. *Nature*, *564*, 99–103. https://doi.org/10.1038/s41586-018-0747-1

Van Damme, M., Erisman, J. W., Clarisse, L., Dammers, E., Whitburn, S., Clerbaux, C., et al. (2015). Worldwide spatiotemporal atmospheric ammonia (NH_3) columns variability revealed by satellite. *Geophysical Research Letters*, *42*(20), 8660–8668. https://doi.org/10.1002/2015gl065496

Van Damme, M., Whitburn, S., Clarisse, L., Clerbaux, C., Hurtmans, D., & Coheur, P.-F. (2017). Version 2 of the IASI NH_3 neural network retrieval algorithm: Near-real-time and reanalysed datasets. *Atmospheric Measurement Techniques*, *10*(12), 4905–4914. https://doi.org/10.5194/amt-10-4905-2017

Viatte, C., Petit, J.-E., Yamanouchi, S., Van Damme, M., Doucerain, C., Germain-Piaulenne, E., et al. (2021). Ammonia and PM2.5 air pollution in Paris during the 2020 COVID lockdown. *Atmosphere*, *12*(2), 160. https://doi.org/10.3390/atmos12020160

Walker, J., Robarge, W., Wu, Y., & Meyers, T. (2006). Measurement of bi-directional ammonia fluxes over soybean using the modified bowen-ratio technique. *Agricultural and Forest Meteorology*, *138*(1–4), 54–68. https://doi.org/10.1016/j.agrformet.2006.03.011

Wang, Q., Zhang, Q., Ma, Z., Ge, B., Xie, C., Zhou, W., et al. (2019). Temporal characteristics and vertical distribution of atmospheric ammonia and ammonium in winter in Beijing. *The Science of the Total Environment*, *681*, 226–234. https://doi.org/10.1016/j.scitotenv.2019.05.137

Wang, S., Nan, J., Shi, C., Fu, Q., Gao, S., Wang, D., et al. (2015). Atmospheric ammonia and its impacts on regional air quality over the megacity of Shanghai, China. *Scientific Reports*, *5*(1). https://doi.org/10.1038/srep15842

Wang, T., Song, Y., Xu, Z., Liu, M., Xu, T., Liao, W., et al. (2020). Why is the Indo-Gangetic Plain the region with the largest NH_3 column in the globe during pre-monsoon and monsoon seasons? *Atmospheric Chemistry and Physics*, *20*(14), 8727–8736. https://doi.org/10.5194/acp-20-8727-2020

Wang, W., Liu, C., Clarisse, L., Van Damme, M., Coheur, P.-F., Xie, Y., et al. (2020). Spatial distribution and seasonal variability in atmospheric ammonia measured from ground-based FTIR observations at Hefei, China. *Atmospheric Measurement Techniques Discussion*. https://doi.org/10.5194/amt-2020-39

Wang, Z., Uno, I., Osada, K., Itahashi, S., Yumimoto, K., Chen, X., et al. (2020). Spatio-temporal variations of atmospheric NH_3 over East Asia by comparison of chemical transport model results, satellite retrievals and surface observations. *Atmosphere*, *11*(9), 900. https://doi.org/10.3390/atmos11090900

Warner, J. X., Dickerson, R. R., Wei, Z., Strow, L. L., Wang, Y., & Liang, Q. (2017). Increased atmospheric ammonia over the world's major agricultural areas detected from space. *Geophysical Research Letters*, *44*(6), 2875–2884. https://doi.org/10.1002/2016gl072305

Warner, J. X., Wei, Z., Strow, L. L., Dickerson, R. R., & Nowak, J. B. (2016). The global tropospheric ammonia distribution as seen in the 13-year AIRS measurement record. *Atmospheric Chemistry and Physics*, *16*(8), 5467–5479. https://doi.org/10.5194/acp-16-5467-2016

Wentworth, G. R., Murphy, J. G., Benedict, K. B., Bangs, E. J., & Collett, J. L., Jr (2016). The role of dew as a night-time reservoir and morning source for atmospheric ammonia. *Atmospheric Chemistry and Physics*, *16*(11), 7435–7449. https://doi.org/10.5194/acp-16-7435-2016

Whitburn, S., Van Damme, M., Clarisse, L., Bauduin, S., Heald, C. L., Hadji-Lazaro, J., et al. (2016). A flexible and robust neural network IASI-NH_3 retrieval algorithm. *Journal of Geophysical Research*, *121*(11), 6581–6599. https://doi.org/10.1002/2016jd024828

Yang, J., Zhang, Z., Wei, C., Lu, F., & Guo, Q. (2017). Introducing the new generation of Chinese geostationary weather satellites, Fengyun-4. *Bulletin of the American Meteorological Society*, *98*(8), 1637–1658. https://doi.org/10.1175/bams-d-16-0065.1

Zhan, X., Adalibieke, W., Cui, X., Winiwarter, W., Reis, S., Zhang, L., et al. (2021). Improved estimates of ammonia emissions from global croplands. *Environmental Science and Technology*, *55*(2), 1329–1338. https://doi.org/10.1021/acs.est.0c05149

Zhang, L., Wright, L. P., & Asman, W. A. H. (2010). Bi-directional air-surface exchange of atmospheric ammonia: A review of measurements and a development of a big-leaf model for applications in regional-scale air-quality models. *Journal of Geophysical Research*, *115*(D20). https://doi.org/10.1029/2009jd013589

Zhang, Q., Yu, Y., Zhang, W., Luo, T., & Wang, X. (2019). Cloud detection from FY-4A's Geostationary Interferometric Infrared Sounder using machine learning approaches. *Remote Sensing*, *11*(24), 3035. https://doi.org/10.3390/rs11243035

Zhang, Y., Dore, A., Ma, L., Liu, X., Ma, W., Cape, J., & Zhang, F. (2010). Agricultural ammonia emissions inventory and spatial distribution in the North China Plain. *Environmental Pollution*, *158*(2), 490–501. https://doi.org/10.1016/j.envpol.2009.08.033

Zhu, L., Henze, D., Bash, J., Jeong, G.-R., Cady-Pereira, K., Shephard, M., et al. (2015). Global evaluation of ammonia bidirectional exchange and livestock diurnal variation schemes. *Atmospheric Chemistry and Physics*, *15*(22), 12823–12843. https://doi.org/10.5194/acp-15-12823-2015